INSTITUTE OF PLASMA PHYSICS

NAGOYA UNIVERSITY

Enhancement of D-T Reaction Rate due to D-T Contact

Shigehisa Hitoki*, Masatada Ogasawara*

and Osamu Aono**

(Received Sept.20 1979)

IPPJ-419 Sept. 1979

RESEARCH REPORT

NAGOYA, JAPAN

Enhancement of D-T Reaction Rate due to D-T Contact

Shigehisa Hitoki*, Masatada Ogasawara*

and Osamu Aono**

(Received Sept.20 1979)

IPPJ-419 Sept. 1979

Further communication about this report is to be sent to the Research Information Center, Institute of Plasma Physics, Nagoya University, Nagoya 464, Japan.

Permanent Address:

* Faculty of Engineering, Keio University,
Hiyoshi, Yokohama 223

**Department of Physics, Jichi Medical School,
Yakushiji, Tochigi 329-04

Abstract

The reaction rate that is appropriate for magnetized nonuniform plasma is numerically calculated to investigate the enhancement of the D-T reaction rate. Spatial separation of the guiding center distributions of D and T enhances the reaction rate. Cases of several guiding center configurations are investigated. The largest enhancement is obtained, when both guiding center distributions are δ-functions which are separated by a length that corresponds to the Gamow peak energy. As compared with the case of no separation of D and T, the maximum enhancing factors obtained are 2.3 for total reaction rate and 1.6 for local reaction rate. Cases of the guiding center distributions with finite widths are also investigated.

§ 1. Introduction

The equilibrium distribution functions for the ionized particles in a magnetized plasma are known to be the local Maxwellian around the guiding center[1]. The guiding center distribution can be taken arbitrarily. Hence strictly speaking, the usual definition of the reaction rate $r=n_D n_T\langle\sigma v\rangle$ does not hold for an inhomogeneous magnetized plasma. Here $\langle\ \rangle$ is the average with respect to the Maxwellian distribution. Using the local Maxwellian distribution, we will define the local reaction rate[2-6] by

$$r(\vec{x}) = \iint d\vec{g}d\vec{G} f_D(\vec{x},\vec{v}_D) f_T(\vec{x},\vec{v}_T)\sigma(g)g \ , \tag{1.1}$$

where $\sigma(g)=A/(\mu g^2/2)\exp(-B/\sqrt{\mu g^2/2})$[3,5,6] is the differential cross section for D-T reaction, $A=1.55\times10^{-20}\mathrm{cm}^2\mathrm{kev}$, $B=34.27\mathrm{kev}^{1/2}$, $\mu=m_D m_T/(m_D+m_T)$ is the reduced mass, and $\vec{G}=(m_D\vec{v}_D+m_T\vec{v}_T)/(m_D+m_T)$ and $\vec{g}=\vec{v}_D-\vec{v}_T$ are respectively the velocity of the center of mass and the relative velocity. If we separate the guiding center distributions of D and T (D-T contact), we will have more head-on collisions and then an enhancement of the reaction rate. By taking several distributions of guiding center, we will calculate the reaction rates and discuss their enhancement. The spatially total reaction rate over the volume of the system and the local reaction rate are considered. The former is enhanced to 2.3 times the total reaction rate for the mixture and the latter 1.6 times. Separation by a length corresponding to Gamow peak energy gives a maximum rate. Recently the migma-cell[7] and the merging tokamak[8], analogous to our D-T contact, have been proposed. In the former the aim is similar to ours, but the mechanism is different. In the latter case, the situation is

similar but the aim is different.

The total and local reaction rates for a model of an axially symmetric D-T contact are given in § 2. In § 3, investigations are made for contact of separated D and T columns. In § 4, cases of the guiding center distributions with finite widths are investigated. Concluding remarks are given in § 5.

§ 2. Axially Symmetric D-T Contact

2.1 Total reaction rate

Here we calculate the total reaction rate

$$J = \int\int d\vec{x} r(\vec{x}), \tag{2.1}$$

for the cylindrically symmetric distributions of D and T. On the X-Y plane in the guiding center space, T is assumed to distribute around the origin and D on a circle of radius R_0 with its center at the origin (Fig.1). The magnetic field $\vec{B}$ is taken along the z-direction. We will take the Gaussians for the guiding center distributions of D and T,

$$f_D(\vec{x},\vec{v}_D) = \frac{\bar{n}}{2} W \exp\{-(\frac{R_D-R_0}{d_D})^2\} F_D(\vec{v}_D) , \tag{2.2}$$

and

$$f_T(\vec{x},\vec{v}_T) = \frac{\bar{n}}{2}(\pi d_T^2)^{-1} \exp\{-(\frac{R_T}{d_T})^2\} F_T(\vec{v}_T) , \tag{2.3}$$

where $\bar{n}$ is the total ion number density per unit length in the z-direction, $R_j=\sqrt{X_j^2+Y_j^2}$, $X_j=x+(v_{jy}/\Omega_j)$, $Y_j=y-(v_{jx}/\Omega_j)$, d_j the width of the guiding center distribution (normalized to be $k_j=d_j/\rho_j$, $\rho_j=v_{thj}/\Omega_j$, $v_{thj}=\sqrt{2T/m_j}$ and $\Omega_j=eB/m_j$), F_j the Maxwellian velocity distribution of j species, and $W^{-1}=\int\int dX_D dY_D \exp[-\{(R_D-R_0)/d_D\}^2]$.

Total reaction rate becomes

$$J(\bar{R}) = \frac{\bar{n}^2}{4}\frac{c_1}{H(\bar{R})}\exp(-\bar{M}\bar{R}^2)\frac{1}{\pi}\int_0^{\pi/2}d\phi\int_0^{\pi/2}d\theta\sin\theta$$

$$\times\int_0^{\infty}dE\exp[-\{1+4\bar{M}'(1-\frac{\bar{M}}{M_T}k_D^2\sin^2\phi)\sin^2\theta\}E-\frac{B'}{\sqrt{E}}$$

$$+4\bar{M}\sin\phi\sin\theta\sqrt{E}]\times\Psi(\bar{R}) , \tag{2.4}$$

where $\bar{M}=M_D M_T/\{(M_D-M_T)^2+M_T k_T^2+M_D k_D^2\}$, $\bar{M}'=\bar{M}$ with $k_D=0$, $M_j=m_j/(m_D+m_T)$, $c_1=2A'\bar{M}v_\mu/\pi^{3/2}\rho_\mu^2$, $A'=A/T$, $\rho_\mu^2=v_\mu^2/\Omega_\mu^2$, $v_\mu^2=2T/\mu$, $\Omega_\mu=eB/\mu$, $B'=B/\sqrt{T}$, $\bar{R}=R_0/\rho_\mu$, $E=\mu g^2/2T$, $d\vec{g}=g^2 dg\sin\theta d\theta d\phi$, and

$$H(\bar{R}) = \exp(-\frac{M_T\bar{R}^2}{k_D^2}) + \frac{\sqrt{\pi}M_T\bar{R}}{k_D}\{1 + Erf(\frac{\sqrt{\pi}M_T\bar{R}}{k_D})\} ,$$

$$Erf(x) = \frac{2}{\sqrt{\pi}} \int_0^x dt\exp(-t^2) ,$$

$$\Psi(\bar{R}) = 2\times\exp(-p_1^2) + \sqrt{\pi}p_1\{1 + Erf(p_1)\}$$

$$+ \sqrt{\pi}p_2\exp(-8\bar{M}\bar{R}\sin\theta\sin\phi\sqrt{E})\{1 \pm Erf(|p_2|)\}. \qquad (2.5)$$

We take the sign $\pm$ in the last term of (2.5) depending on $p_2 \gtrless 0$ and

$$\begin{bmatrix} p_1 \\ p_2 \end{bmatrix} = (\frac{M_T\bar{M}}{\bar{M}'k_D^2})^{1/2}\bar{R}\begin{bmatrix} + \\ - \end{bmatrix} 2(\frac{\bar{M}\bar{M}'}{M_T})^{1/2}k_D\sqrt{E}\sin\theta\sin\phi .$$

In the limit $k_D\to 0$, eq.(2.4) reduces to

$$J(\bar{R}) = \frac{\bar{n}^2}{4} c_1 \exp(-\bar{M}'\bar{R}^2) \int_0^{\pi/2} d\theta\sin\theta$$

$$\times \int_0^\infty dE\exp\{-(1+4\bar{M}\sin^2\theta)E - \frac{B'}{\sqrt{E}}\} I_0(4\bar{M}'\bar{R}\sin\theta\sqrt{E}) ,$$

(2.6)

where I_0 is the 0-th order modified Bessel function, and the limit $k_T\to 0$ corresponds to $\bar{M}'\to\bar{M}''=M_D M_T/(M_T-M_D)^2$ in (2.6).

2.2 Local reaction rate and reaction probability

Assuming δ-functions for the guiding center distributions of D and T, we have for the local reaction rate (1.1)

$$r(\bar{R},\bar{r}) = \frac{\bar{n}^2}{4} c_2 \exp\{-M_D M_T(\bar{R}^2+4\bar{r}^2)\} \times \int_0^{\pi} \frac{d\phi}{\pi} \exp(4M_D M_T \bar{r}\bar{R}\cos\phi) \int_0^{\infty} dg_z g^{-1} \exp(-g^2 - \frac{B'}{g}) , \tag{2.7}$$

where $g^2=g_z^2+M_T^2\bar{R}^2-2M_T(M_T-M_D)\bar{r}\bar{R}\cos\phi+(M_T-M_D)^2\bar{r}^2$, $c_2=2M_D M_T A' v_\mu/\pi^{5/2}\rho_\mu^4$ and $\bar{r}=r/\rho_\mu$. In this case, the number densities of D and T are

$$n_D(\bar{R},\bar{r}) = \frac{\bar{n}}{2}(\pi\rho_D^2)^{-1}\exp\{-M_T(\bar{R}^2+\bar{r}^2)\} I_0(2M_T\bar{R}\bar{r}) , \tag{2.8}$$

and

$$n_T(\bar{r}) = \frac{\bar{n}}{2}(\pi\rho_T^2)^{-1}\exp(-M_D\bar{r}^2) . \tag{2.9}$$

We will define the reaction probability by

$$\langle\sigma g\rangle_A = \frac{r(\bar{R},\bar{r})}{n_D(\bar{R},\bar{r})n_T(\bar{r})} . \tag{2.10}$$

2.3 Numerical results and discussions

We will numerically evaluate the total reaction rate (2.6) and the local reaction probability (2.10). Since the integrands of (2.6) and (2.10) are broad, we cannot use the "sattelpunktmethode".

The total reaction rate $J(\bar{R})$, given in Fig.2, has a maximum for certain $\bar{R}$ that corresponds to the gyro-radius of a triton with the Gamow peak energy[4] $W_m=6.6T_k^{2/3}$ (T_k is the kinetic temperature in kev unit). From this expression the relative velocities at Gamow peak are given by $g_m\simeq 3.9v_{thT}$ and $3.1v_{thT}$, respectively for $T_k=1.2$ and 5. These velocities correspond to $\bar{R}=3.9$ and 3.1, which agree with the results of Fig.2. The maximum values of $J(\bar{R})/J(0)$ are 2.3, 1.7 and 1.6, respectively for $T_k=1.2$, 5 and 10. Separation of D and T distributions gives the increase of relative velocity, which corresponds to an increase of effective temperature. The reaction cross-section σ has larger derivatives $d\sigma/dE$ at low energy. Then $J(\bar{R})/J(0)$ due to D-T contact is larger in the lower temperature case ($T_k=1.2$). It is confirmed that δ-functions for the guiding center distributions ($k_D=k_T=0$) give the largest $J(\bar{R})/J(0)$ under the same physical conditions. This is because the chance of head-on collision is largest in the case of $k_D=k_T=0$. As the width of the guiding center distribution increases, the given D-T system approaches to the system of spatially uniform mixture and then the chance of head-on collision decreases. In Fig.3, the reaction probability $\langle\sigma g\rangle_A$ are shown as a function of $\bar{r}=r/\rho_\mu$ taking $\bar{R}=R_0/\rho_\mu$ as a parameter. It can be shown that each curve in Fig.3 has its minimum around $\bar{r}\simeq 3\bar{R}$, where the relative velocity becomes

minimum, and that the curves intersect. Larger $\bar{R}$ corresponds to larger reaction probability as far as $\bar{r}<3\bar{R}$. Owing to this fact, the total reaction rate increases with the increase of $\bar{R}$. In Fig.4, value of $\langle\sigma g\rangle_A$ at $\bar{r}=0$ is shown as a function of $\bar{R}$. Next we will consider the relation between the local and the total reaction rates. The product $n_D n_T$ has a maximum at $\bar{r}\simeq\bar{R}/2$, so that the local reaction rate also becomes maximum. This maximum value decreases monotonically as $\bar{R}$ increases, because $n_D n_T$ decreases sharply as $\bar{R}$ increases. From this, there seems to be no merit for the local reaction rate $r(\bar{R},\bar{r}=\bar{R}/2)$. However, it holds $r(3<\bar{R}<4,\ \bar{r}>1)>r(\bar{R}=0,\ \bar{r}>1)$, where the region $3<\bar{R}<4$ corresponds to the case that gives the maximum for the total reaction rate. Hence the total reaction rate, which is an integral of the local reaction rate, is enhanced when $\bar{R}\neq 0$.

§ 3. Contact of D and T Columns

3.1 Local reaction rate

We will take the distribution functions for D and T

$$f_D(\vec{x},\vec{v}_D) = \frac{\bar{n}}{2}\,\delta(X_D+X_0)\delta(Y_D)F_D(\vec{v}_D)\ , \tag{3.1}$$

and

$$f_T(\vec{x},\vec{v}_T) = \frac{\bar{n}}{2}\,\delta(X_T-X_0)\delta(Y_T)F_T(\vec{v}_T)\ . \tag{3.2}$$

Since the guiding centers of D and T are located at the points, $X=\pm X_0$ and $Y=0$, D and T columns are in contact in real space. For the total reaction rate, we obtain the same expression as (2.6) with $k_D=k_T=0$ and $\bar{R}/2$ replaced by $\bar{X}=X_0/\rho_\mu$. For the local reaction rate at x=y=0 we have

$$r(\bar{X}) = \frac{\bar{n}^2}{4}\,c_2\int_0^\infty dg_z\, g^{-1}\exp(-g^2-\frac{B'}{g})\ , \tag{3.3}$$

where $g^2=g_z^2+\bar{X}^2$. Number densities n_j for j=D and T at x=y=0 are

$$n_j(\bar{X}) = \frac{\bar{n}}{2}(\pi\rho_j^2)^{-1}\exp\{-(\frac{X_0}{\rho_j})^2\}\ . \tag{3.4}$$

The reaction probability for the present case is given by $\langle\sigma g\rangle_B = r(\bar{X})/n_D(\bar{X})n_T(\bar{X})$.

3.2 Numerical results and discussions

Both the axially symmetric D-T contact (treated in §2) and the contact of separated D and T columns (present section) give the same total reaction rate when we put $\bar{R}/2=\bar{X}$. Collision between a triton, at the center of a circle of radius $\bar{R}$ (Fig.1), and a deuteron at a point A on the circle is completely equivalent to the collision between the triton and a deuteron at some other point B on the circle. As far as D-T reaction concerns, the above two collisions are independent. So even if we bring the deuteron on the point B to the point A together, the total number of collisions does not change. Then the case of distributed deuterons on the circle is equivalent to the case of concentrated deuterons on a point, which is the present case of columns.

The local reaction probability (3.4) and the local reaction rate (3.3) for $T_k=5$ are shown in Fig.4 and 5 respectively. As $\bar{X}$ increases, i.e., as D and T columns separate, the reaction probability $\langle\sigma g\rangle_B$ increases and the local reaction rate $r(\bar{X})$ has a peak. The reaction probability $\langle\sigma g\rangle_B$ is less than $\langle\sigma g\rangle_A$ at $\bar{r}=0$ in the cylindrical case. However, in the present case, the local reaction rate is enhanced because the number densities of D and T decrease more moderately than in the cylindrical case as $\bar{X}$ or $\bar{R}$ increases. The maximum enhancement is 1.6 times the usual mixture at $2\bar{X}\simeq 10$ for $T_k=5$.

§ 4. Contact of D and T Slabs

In the preceding sections, we have investigated the case of δ-function distributions of D and T guiding centers. Here we will study the cases of the guiding center distributions with finite widths.

The guiding centers are assumed to exist on a sheet at Y=0. Then D and T distribute in slab-like geometry. We will consider three cases (C)-(E), of which guiding center distributions N(X) are given in Fig.6. In the z-direction, infinity and homogeneity are assumed. The distribution functions and the expressions of the local reaction rates at x=y=0 calculated with use of them are given in Table 1 and 2. In Figs.7(a) and 7(b), numerical results r_C, r_D and r_E are presented for T_k=5 and 20, respectively, and for B=1Wb/m^2. The width L is normalized by $L_G=2\sqrt{6.6}T_k^{-1/6}\rho_\mu$, which is the gyro-radius of a particle with the reduced mass μ, gyrating with the Gamow energy[4] $W_m=6.6T_k^{2/3}$. To increase the width L, keeping the number density of the guiding centers at X=0 constant, corresponds to the increase of the total number of the guiding centers.

For both temperature cases, it follows that $r_C<r_D<r_E$. This is reasonable, since in the model (E) the number of head-on collision between D and T is the largest. As L increases infinitely, the graphs of r_C and r_D approaches to the dotted lines, which corresponds to the case of uniform D-T mixture, and r_E saturates. The rate r_D has a broad maximum around $L/2\simeq L_G$. Other two cases (C) and (E) give no maxima, as it should. Though the absolute values of the reaction rates are smaller in low temperature case (5kev), the ratios r_D/r_C and r_E/r_C are larger as seen in Fig.8. Since the reaction

cross-section is a steep increasing function of energy in low energy region and as the width L increases, the distribution f is broadened, the product fσg, hence the reaction rate, is more enhanced at lower temperature when L increases. The ratios r_D/r_C and r_E/r_C becomes 5.5 and 7.4, respectively, at $L/L_G=1.5$ for $T_k=5$.

If the guiding centers distribute uniformly in the Y-direction, the inequality $r_C'<r_D'<r_E'$ also holds. Here primes mean corresponding reaction rates to the cases (C)-(E). As shown in Fig.8, ratios r_D'/r_C' and r_E'/r_C' decrease as compared with r_D/r_C and r_E/r_C. This is because the system approaches to three dimensional uniform one, by extending the sheet distribution at Y=0 uniformly into Y-direction.

We have also investigated the cases (D) and (D') in decreasing L, originally taken larger than L_G, keeping the total number of the guiding centers constant. The reaction rate r_D has a maximum near $L\simeq L_G$ which is analogous to the case of δ-function distribution (Fig.5). And r_D' approaches to the limiting value r_C in the limit of $L\to\infty$, as it should.

§ 5. Concluding Remarks

We have considered the enhancement of the reaction rate by D-T contact in strong magnetic field. The reaction rate is mainly determined by the area around Gamow peak in energy space. Therefore, our purpose has been to seek the guiding center profiles that result in a large fraction of particles having energy near Gamow peak. The guiding centers of colliding particles should be separated. The separation must be optimum when it corresponds to Gamow peak energy. From this physical picture, we have proposed the D-T contact for the enhancement of the reaction rate.

In the axially symmetric case in §2, the total reaction rate has increased 1.7 times that of the usual mixture for $T_k=5$. The local reaction probability has been remarkably enhanced. However, here we must note that the number densities of D and T sharply decrease in D-T contact. In §3, the contact of D and T columns has been investigated. The total reaction rate has given the same expression as that in the axially symmetric case. The local reaction probability has also been remarkably enhanced and we have obtained an enhancing factor 1.6 for the local reaction rate when $T_k=5$. This is in contrast to the result of §2. It is because the number densities of D and T have decreased moderately.

In §4, the local reaction rate r_C, r_D and r_E have been treated in the cases that the guiding center distributions of D and T have finite widths in the X-direction and form a sheet in the Y-direction. In §4, the number densities of D and T of all the models (C)-(E) are taken to be the same at the position where we have estimated the local reaction rates,

which is different from §2 and §3. A comparison has been made between r_E and r_C. In case (E), only the head-on collisions occur. Case (C) corresponds to a uniform mixture. The ratio r_E/r_C has become 7.4 for T_k=5. However one should notice that the contact of D and T columns (the case of δ-function) gives larger reaction rate than the case (E), if the total number of the guiding centers is the same.

Our D-T contact can be realized without external source such as T.C.T.[9,10].

Acknowledgements

The authors wish to express their deep gratitude to Prof.S.Kaneko, Department of Applied Physics, University of Tokyo, for valuable discussions and suggestions given during the course of the work.

They are also grateful to Dr.M.Sugihara, Division of Large Tokamak Development, Japan Atomic Energy Research Institute, for helpful discussions and suggestions.

References

(1) T.Kihara, Y.Midzuno and S.Kaneko: J.Phys.Soc.Japan 15 (1960)1101.

(2) K.Sakai and O.Aono: J.Phys.Soc.Japan 43(1977)222.

(3) W.B.Thompson: Proc.Phys.Soc. 70B. LXX(1957)1.

(4) J.D.Lawson: ibid. 70B. LXX(1957)6.

(5) L.A.Artsimovich: Controlled Thermonuclear Reactions(Gordon and Breach Science Publishers, New York, 1964)Chap.1.

(6) S.Glasstone and R.H.Lovberg: Controlled Thermonuclear Reactions(Van Nostrand, New York, 1960)Chap.2.

(7) B.Mäglich: Nuclear Instruments and Methods III(North Holland, 1973)213.

(8) V.D.Shafranof: Nuclear Fusion 19(1979)187.

(9) J.M.Dawson, H.P.Furth and F.H.Tenny: Phys.Rev.Lett. 26 (1971)1156.

(10) D.L.Jassby: Nuclear Fusion 17(1977)309.

Figure Captions

Fig.1 The guiding center region (upper), and the number densities of D and T (lower), for the axially symmetric D-T contact.

Fig.2 The total reaction rates $J(\bar{R})$ normalized by $J(0)$ as a function of $\bar{R}=R_0/\rho_\mu$. Temperatures, T_k=1.2, 5 and 10 are used as parameters. The widths of the guiding center distributions of D and T are taken as $k_D=k_T=0$.

Fig.3 For the axially symmetric D-T contact the local reaction probability $\langle\sigma g\rangle_A(\bar{R},\bar{r})$ normalized by $\langle\sigma g\rangle_A(0,0)=2.8\times10^{-18}\mathrm{cm}^3\mathrm{sec}^{-1}$ as a function of $\bar{r}=r/\rho_\mu$. Temperature T_k=5 and parameter is $\bar{R}=R_0/\rho_\mu$.

Fig.4 For the axially symmetric D-T contact, $\log[\langle\sigma g\rangle_A(\bar{R})/\langle\sigma g\rangle_A(0)]$ at $\bar{r}=0$ as a function of $\bar{R}$ and for the contact of D and T columns, $\log[\langle\sigma g\rangle_B(\bar{X})/\langle\sigma g\rangle_B(0)]$ at x=y=0 (dotted line) as a function of $\bar{X}$. Temperature T_k=5 and $\langle\sigma g\rangle_A(0)=\langle\sigma g\rangle_B(0)=2.8\times10^{-18}\mathrm{cm}^3\mathrm{sec}^{-1}$.

Fig.5 For the contact of D and T columns, the local reaction rate at x=y=0, $r(\bar{X})$, normalized by $r(0)$, as a function of $\bar{X}=X_0/\rho_\mu$. Temperature T_k=5 and $r(0)=(\bar{n}^2/4)\times9.5\times10^{-18}$ $\mathrm{cm}^{-3}\mathrm{sec}^{-1}$.

Fig.6 The guiding center distributions of D and T for the cases (C)-(E) as a function of X.

Fig.7 The local reaction rates $r(\bar{L})/(\bar{n}^2/4)$ at x=y=0 as a function of $\bar{L}=L/L_G$ for T_k=5(a) and 20(b) for the cases (C)-(E).

Fig.8 Ratios r_D/r_C, r_E/r_C, r_D'/r_C' and r_E'/r_C' as a function of $\bar{L}=L/L_G$. Solid curves show r_E/r_C and r_E'/r_C'

while dotted ones r_D/r_C and r_D'/r_C'. Left ordinate is used for r_D/r_C and r_E/r_C. Right for r_D'/r_C' and r_E'/r_C'. Temperatures T_k=5 and 20 are taken.

Table 1 Distribution functions of D and T and the local reaction rates at x=y=0 for the cases (C)-(E).

Table 2 Notations in Table 1.

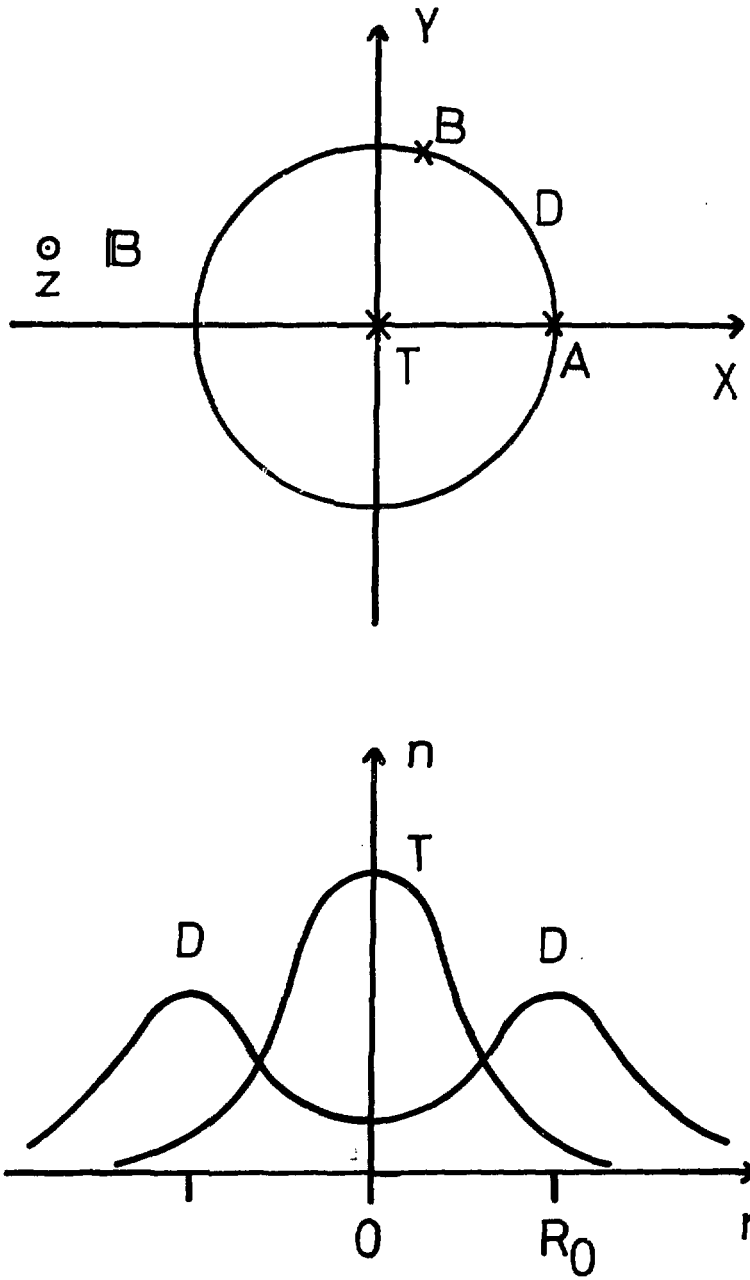

FIG.1

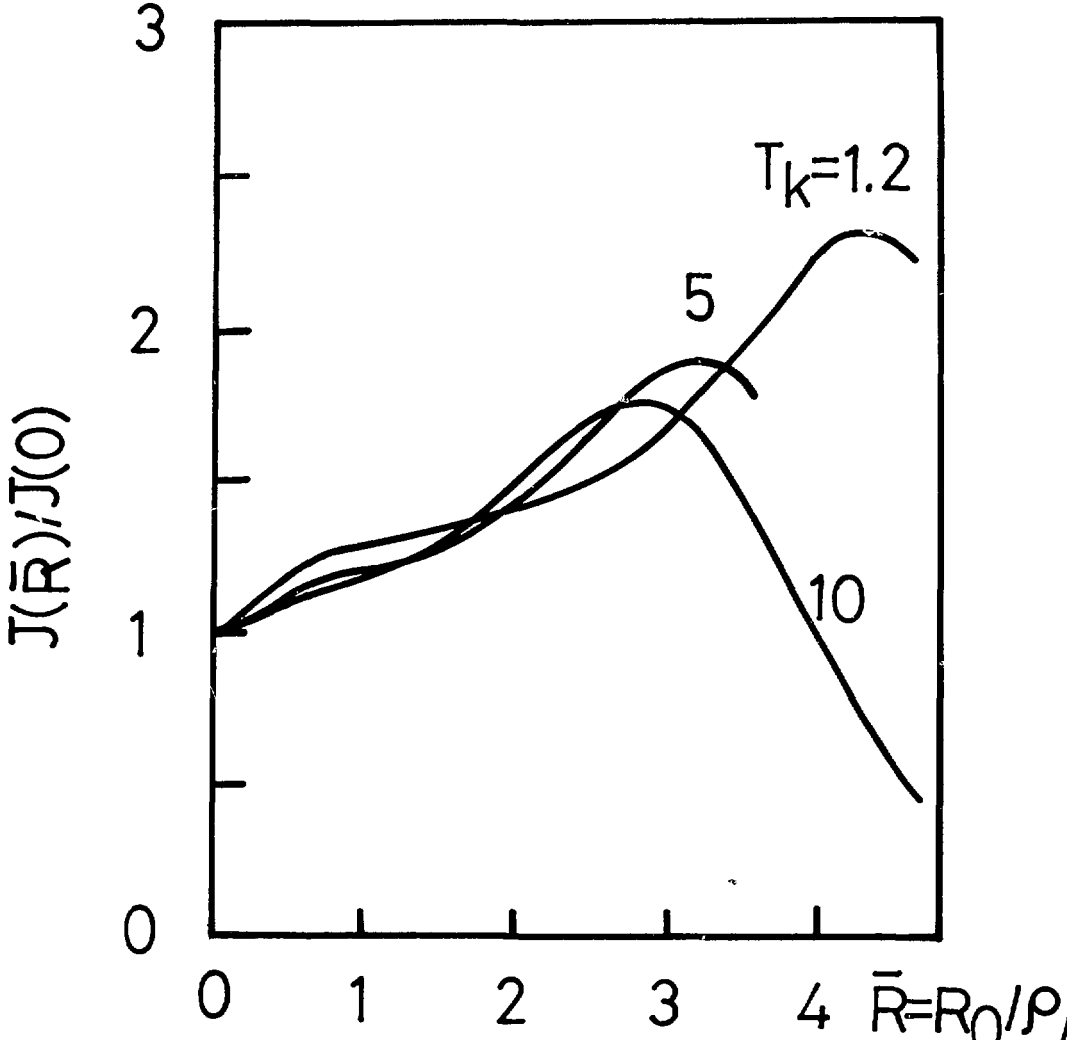

FIG.2

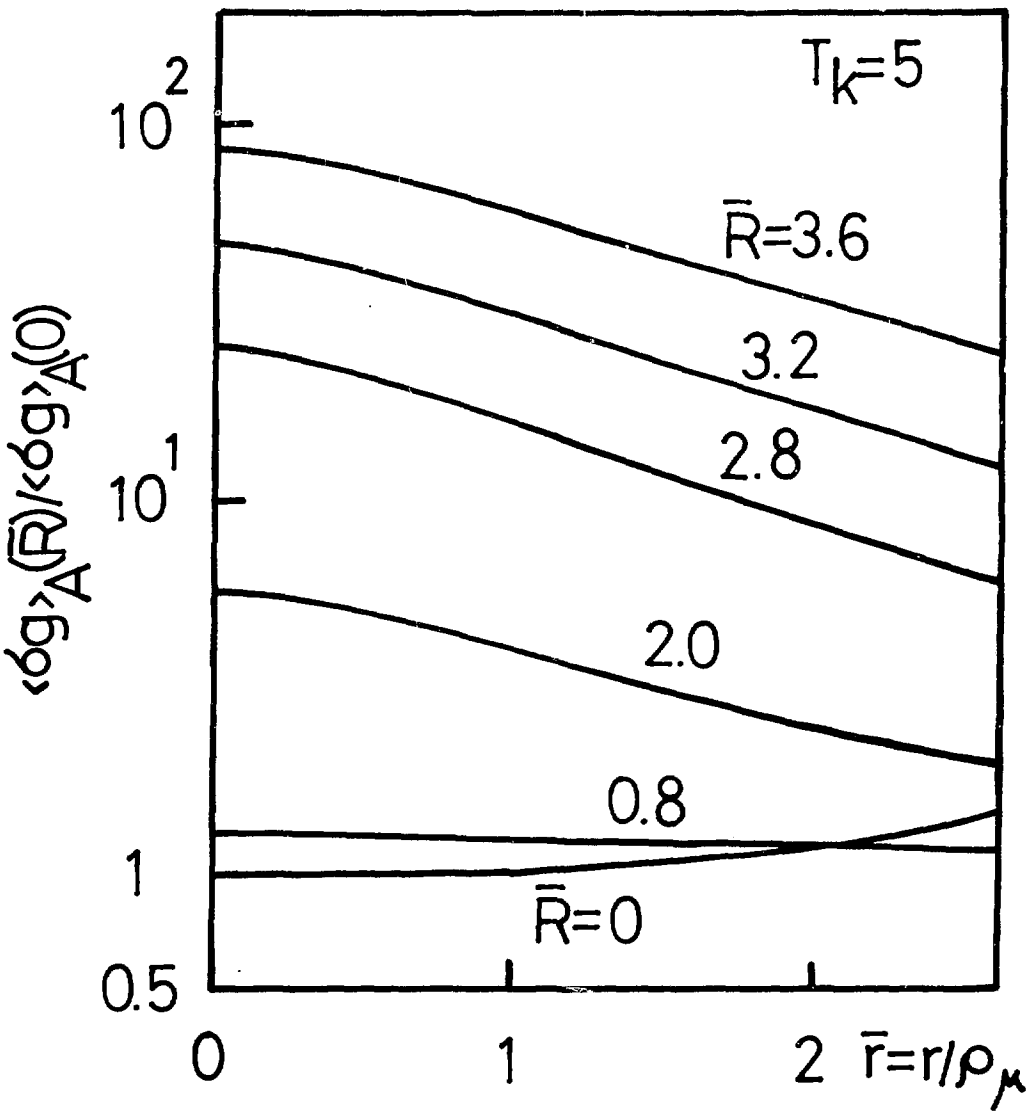
T_k=5
10^2
10^1
1
0.5
$\bar{R}$=3.6
3.2
2.8
2.0
0.8
$\bar{R}$=0
$\langle\delta g\rangle_A(\bar{R})/\langle\delta g\rangle_A(0)$
0
1
2
$\bar{r}=r/\rho_\mu$

FIG.3

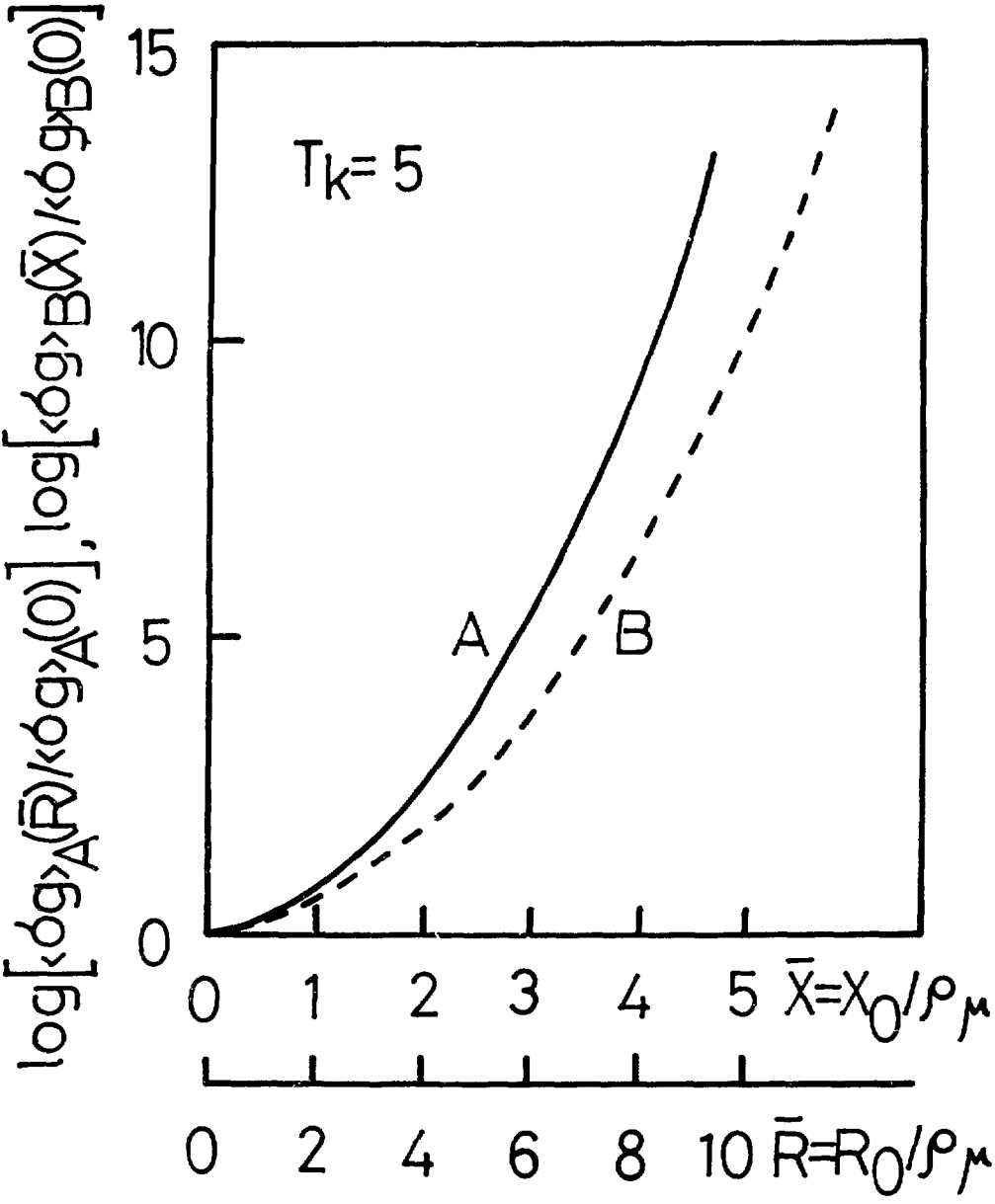
log[⟨δg⟩A(R̄)/⟨δg⟩A(0)], log[⟨δg⟩B(X̄)/⟨δgB(0)]
15
10
5
0
Tk= 5
A
B
0 1 2 3 4 5 X̄=X0/ρM
0 2 4 6 8 10 R̄=R0/ρM

FIG.4

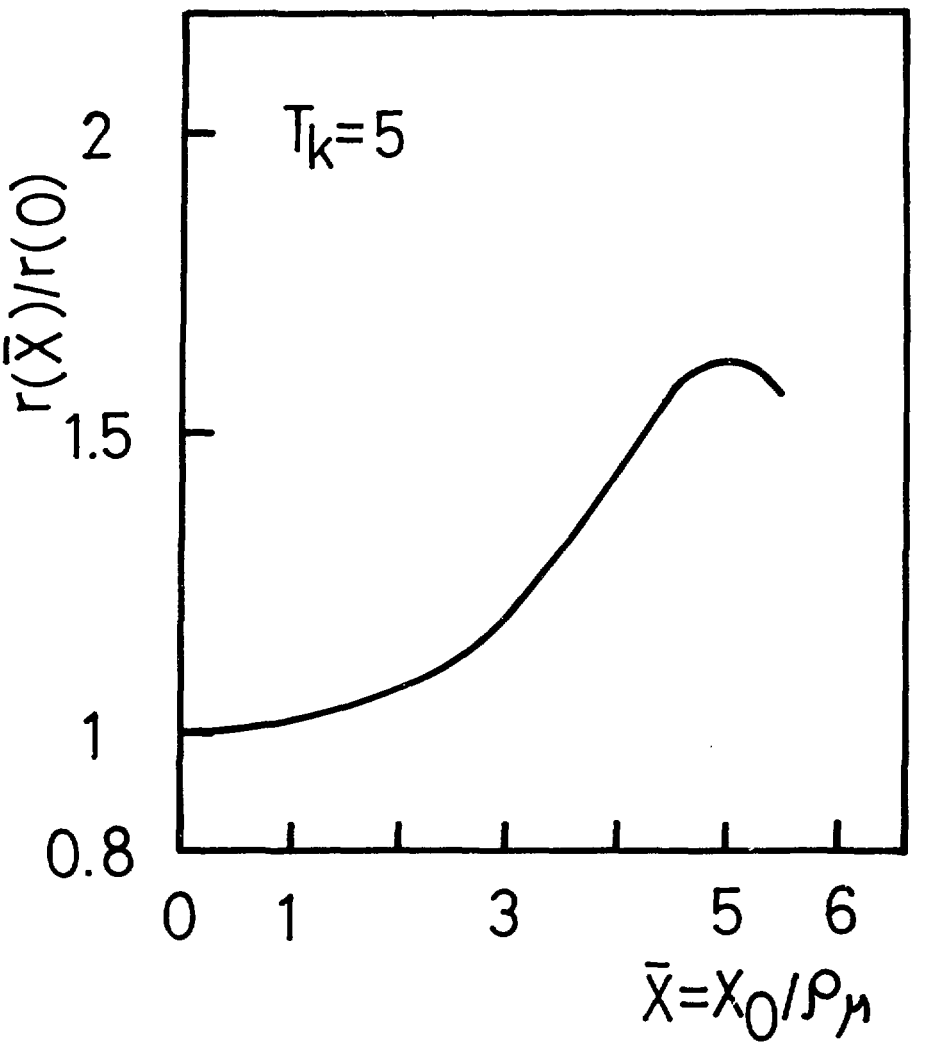

FIG.5

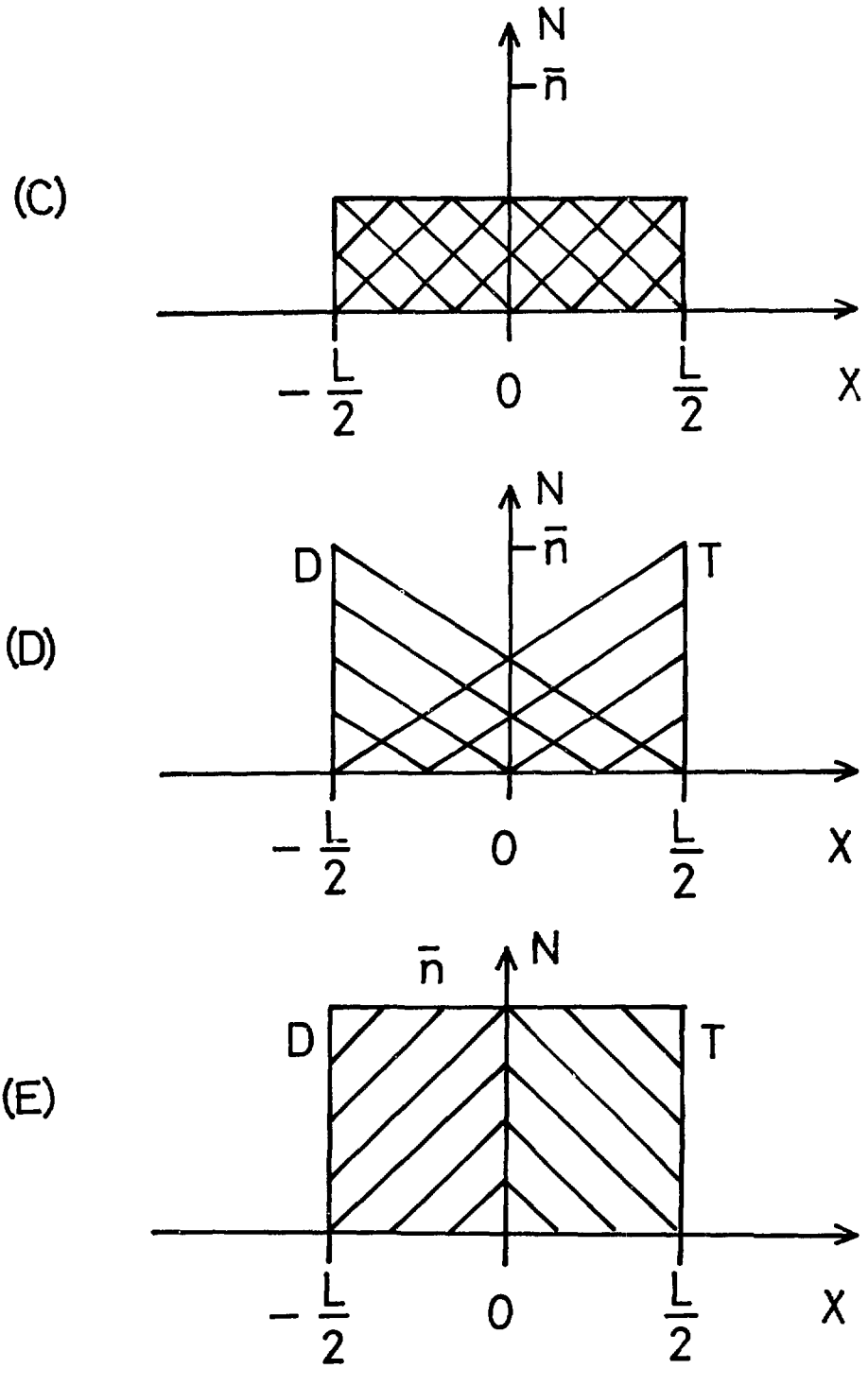

FIG.6

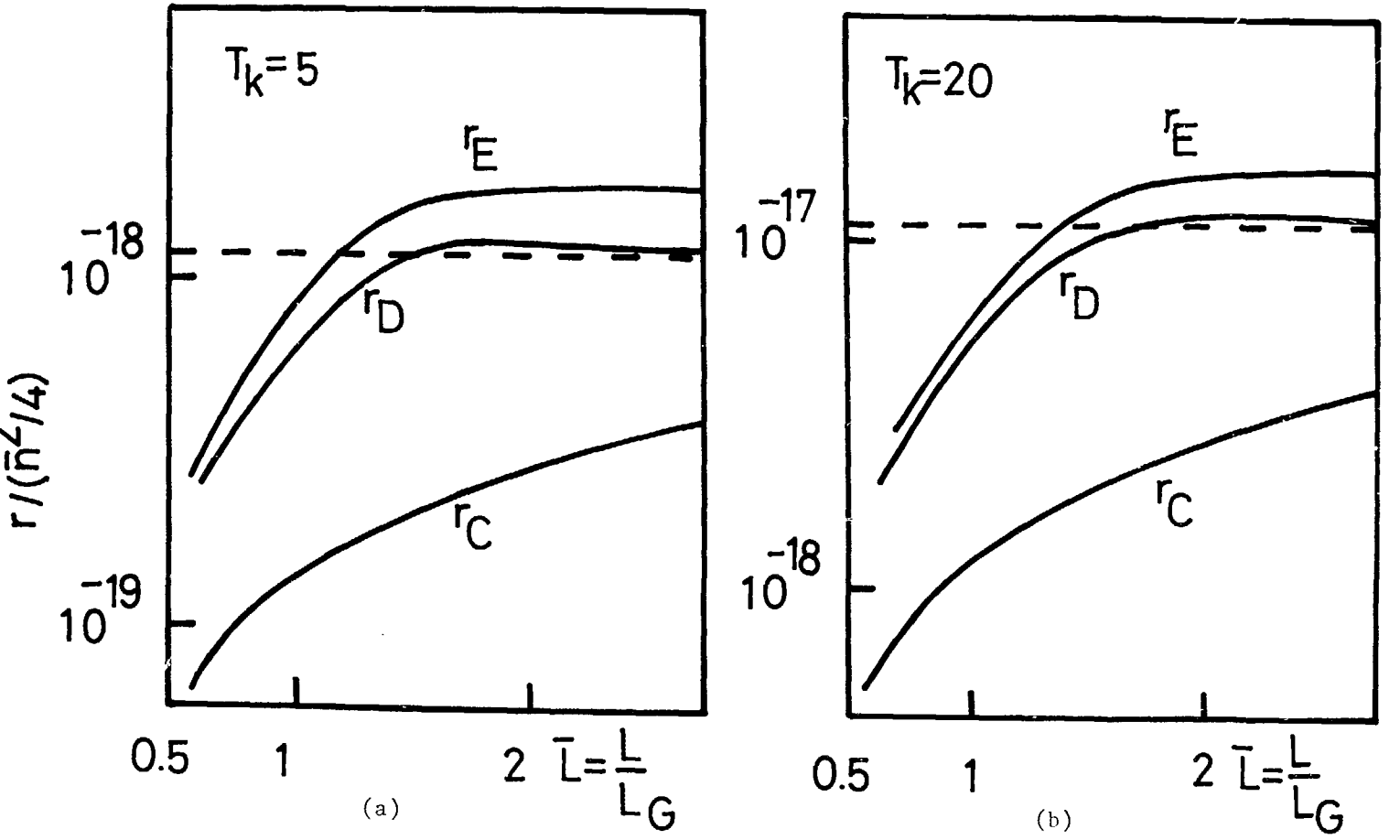
$T_k=5$
r_E
r_D
r_C
10^{-18}
10^{-19}
$r/(\bar{n}^2/4)$
0.5
1
2
$\bar{L}=\frac{L}{L_G}$
(a)
$T_k=20$
r_E
r_D
r_C
10^{-17}
10^{-18}
0.5
1
2
$\bar{L}=\frac{L}{L_G}$
(b)

FIG.7

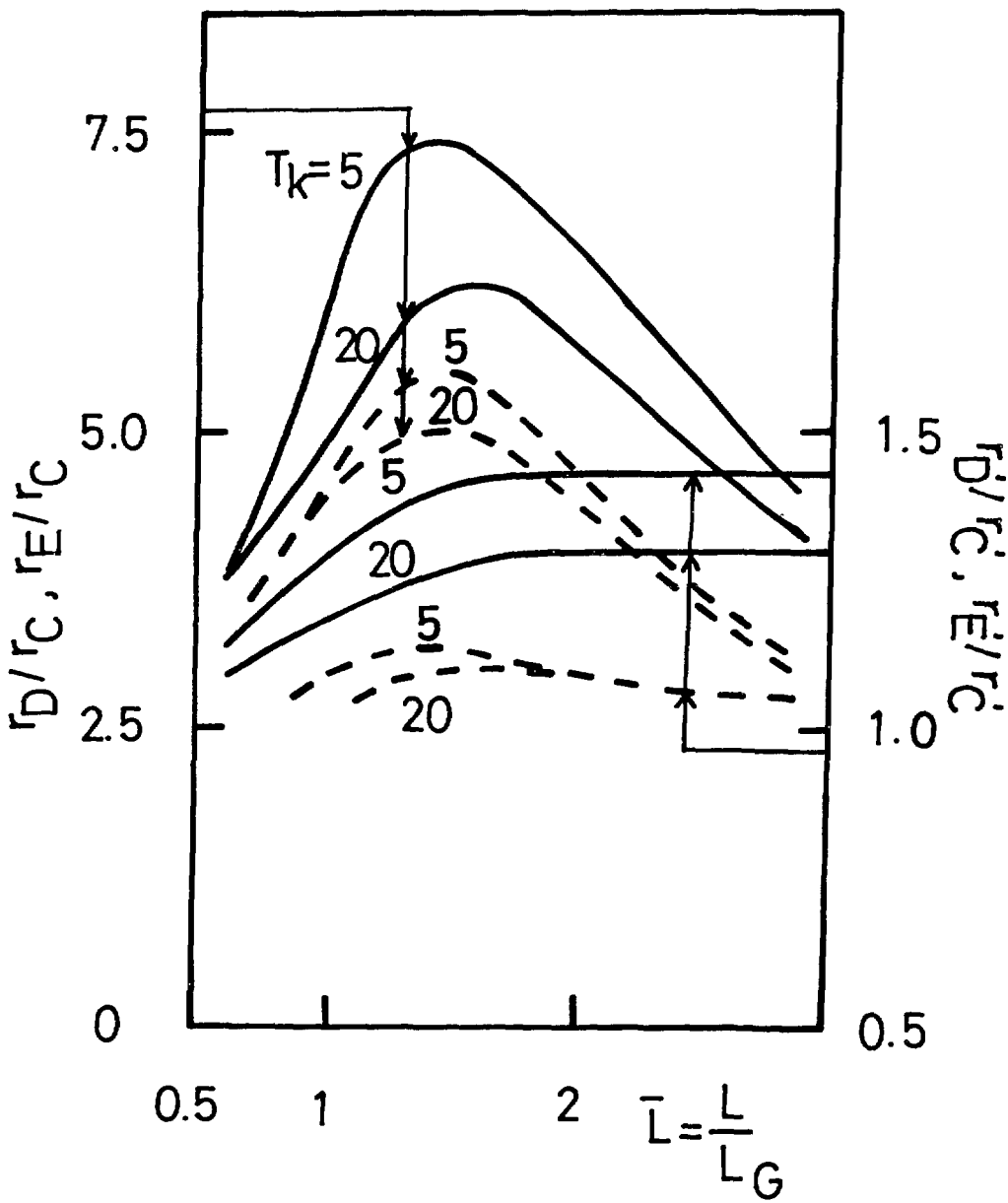
7.5
5.0
2.5
0
1.5
1.0
0.5
T_k=5
20
5
20
5
20
5
20
r_D/r_C, r_E/r_C
r_D/r_C, r_E/r_C
0.5
1
2
$\bar{L}=\frac{L}{L_G}$

FIG. 8

Table 1

(C): $f_j = \frac{\bar{n}}{2}\delta(Y_j)F_j(\vec{v}_j)$ for $|X_j| \leqq L/2$, $j=D$ and T

$$r_C = \frac{\bar{n}^2}{4}c_3\left[\int_{(M_T-M_D)\bar{L}}^{\bar{L}} dg_y\{H_1(g_y)+H_2(g_y)\} + \int_{-(M_T-M_D)\bar{L}}^{(M_T-M_D)\bar{L}} dg_y H_3(g_y)\right]\int_0^\infty dg_z\, g^{-1}\exp\left(-\frac{B'}{g}-g^2\right)$$

(D): $f_D = \frac{\bar{n}}{2}\left(1-\frac{2}{L}X_D\right)\delta(Y_D)F_D(\vec{v}_D)$

$f_T = \frac{\bar{n}}{2}\left(1+\frac{2}{L}X_T\right)\delta(Y_T)F_T(\vec{v}_T)$ for $|X_j| \leqq L/2$

$$r_D = \frac{\bar{n}^2}{4}c_4\int_0^{\sqrt{M_D/M_T(1+M_D^2)}\bar{L}} dG_y'' \int_0^\infty dg_z \int_{-\sqrt{M_DM_T}(1-M_DM_T)G_y''}^{M_T\sqrt{1+M_D^2}\bar{L}-\sqrt{M_DM_T}(1-M_DM_T)G_y''} dg_y'' \times$$

$$\times F_1^{-1/2}\exp\left(-\frac{B'}{\sqrt{F_1}}-F_1-F_2\right)\left\{1-\frac{a_1 g_y''}{\bar{L}}+\frac{a_2 G_y''}{\bar{L}}-\frac{4F_3}{\bar{L}^2}\right\}$$

(E): $f_j = \bar{n}\delta(Y_j)F_j(v_j)$ for $0 \leqq X_D \leqq L/2$ and $-L/2 \leqq X_T \leqq 0$

$$r_E = \bar{n}^2 c_3\left\{\int_{M_T\bar{L}}^{\bar{L}} dg_y H_1(g_y) + \int_{M_D\bar{L}}^{M_T\bar{L}} dg_y H_4(g_y) + \int_0^{M_D\bar{L}} dg_y H_5(g_y)\right\}$$

$$\times\int_0^\infty dg_z\, g^{-1}\exp\left(-\frac{B'}{g}-g^2\right)$$

Table 2

$$c_3=\sqrt{M_D M_T}A' v_\mu / 2\pi^2 \rho_\mu^2,\quad g^2=(\frac{g_y}{2})^2+g_z^2,\quad \tilde{L}=L/\rho_\mu$$

$$H_1(g_y)=Erf\{\frac{1}{2}\sqrt{\frac{M_D}{M_T}}(\tilde{L}-g_y)\}+Erf\{\frac{1}{2}\sqrt{\frac{M_T}{M_D}}(\tilde{L}-g_y)\}$$

$$H_2(g_y)=Erf\{\frac{1}{2}\sqrt{\frac{M_D}{M_T}}(\tilde{L}+g_y)\}+Erf\{\frac{1}{2}\sqrt{\frac{M_T}{M_D}}(\tilde{L}+g_y)\}$$

$$H_3(g_y)=Erf\{\frac{1}{2}\sqrt{\frac{M_D}{M_T}}(\tilde{L}-g_y)\}+Erf\{\frac{1}{2}\sqrt{\frac{M_D}{M_T}}(\tilde{L}+g_y)\}$$

$$H_4(g_y)=Erf\{\frac{1}{2}\sqrt{\frac{M_D}{M_T}}(\tilde{L}-g_y)\}+Erf(\frac{1}{2}\sqrt{\frac{M_D}{M_T}}g_y)$$

$$H_5(g_y)=Erf(\frac{1}{2}\sqrt{\frac{M_T}{M_D}}g_y)+Erf(\frac{1}{2}\sqrt{\frac{M_D}{M_T}}g_y)$$

$$Erf(x)=\frac{2}{\sqrt{\pi}}\int_0^x dt\exp(-t^2)$$

$$c_4=\sqrt{M_D M_T}2A' v_\mu/\pi^{5/2}\rho_\mu^2,\quad a_1=2/M_T\sqrt{1+M_D^2},$$
$$a_2=2(M_T-M_D+2M_D^2M_T)/\sqrt{M_D M_T(1+M_D^2)}$$

$$F_1(g_y'',G_y'')=(\frac{g_y''}{\sqrt{1+M_D^2}}-\frac{M_D\sqrt{M_D M_T}G_y''}{\sqrt{1+M_D^2}}-\frac{M_T-M_D}{2}\tilde{L})^2+g_z^2$$

$$F_2(g_y'',G_y'')=(\sqrt{\frac{M_D}{M_T(1+M_D^2)}}g_y''+\frac{1}{\sqrt{1+M_D^2}}G_y''-\sqrt{M_D M_T}\tilde{L})^2$$

$$F_3(g_y'',G_y'')=b_2G_y''^2+b_3g_y''G_y''+b_4g_y''+b_5G_y''+\frac{\tilde{L}^2}{4}$$

$$b_2=1-M_D M_T,\quad b_3=1/\sqrt{M_D M_T},\quad b_4=-1/2M_T\sqrt{1+M_D^2},\quad b_5=-1/2\sqrt{M_D M_T(1+M_D^2)}$$